JCI insight

Distinctive lipid signatures of bronchial epithelial cells associated with cystic fibrosis drugs, including Trikafta

Nara Liessi, … , Nicoletta Pedemonte, Andrea Armirotti

JCI Insight. 2020. https://doi.org/10.1172/jci.insight.138722.

Research In-Press Preview **Cell biology**

Over the last years, a number of drugs have been approved for the treatment of cystic fibrosis (CF). Among them, the new Trikafta, a combination of three drugs, holds great promises to radically improve the quality of life for a large part of CF patients carrying one copy of the most frequent CFTR mutation: F508del. Currently available, disease-modifying, CF drugs work by rescuing the function of mutated CFTR (Cystic Fibrosis Transmembrane Conductance Regulator) anion channel. Recent research work shows that membrane lipids, and the cell lipidome in general, play a significant role in the mechanism of CFTR defective trafficking and, on the other hand, in its rescue. In this paper, by using untargeted lipidomics on CFBE41o$^-$ cells, we identified distinctive changes in bronchial epithelial cell lipidome associated with treatment with the triple combination VX-661/VX-445/VX-770 (drug name: Trikafta) and other CF drugs. Particularly interesting is the reduction of ceramide levels, known molecular players in the induction of apoptosis, that appears to be associated with a decrease in cell susceptibility to undergo apoptosis. This evidence could account for additional beneficial role of the triple combination on CF phenotypes.

DISTINCTIVE LIPID SIGNATURES OF BRONCHIAL EPITHELIAL CELLS ASSOCIATED WITH CYSTIC FIBROSIS DRUGS, INCLUDING TRIKAFTA

Authors: Nara Liessi[1§], Emanuela Pesce[2§], Clarissa Braccia[3], Sine Mandrup Bertozzi[1], Alessandro Giraudo[3], Tiziano Bandiera[3], Nicoletta Pedemonte[2,#] and Andrea Armirotti[1,#]

Affiliations: 1) Analytical Chemistry Lab, Istituto Italiano di Tecnologia, Via Morego 30, 16163, Genova, Italy; 2) UOC Genetica Medica, IRCCS Giannina Gaslini, Via Gerolamo Gaslini 5, 16147 Genova, Italy; 3) D3PharmaChemistry, Istituto Italiano di Tecnologia, Via Morego 30, 16163, Genova, Italy

§equal contribution

#Shared Correspondence

*To whom correspondence should be addressed:

Andrea Armirotti

Fondazione Istituto Italiano di Tecnologia, Via Morego 30, 16163 Genova, Italy

Tel: +390102896938

andrea.armirotti@iit.it

Nicoletta Pedemonte

UOC Genetica Medica, IRCCS Giannina Gaslini, Via Gaslini 5, 16147 Genova, Italy

Tel: +3901056363178

nicolettapedemonte@gaslini.org

Conflict of Interest

The authors have declared that no conflict of interest exists

Abstract

Over the last years, a number of drugs have been approved for the treatment of cystic fibrosis (CF). Among them, the new Trikafta, a combination of three drugs, holds great promises to radically improve the quality of life for a large part of CF patients carrying one copy of the most frequent CFTR mutation: F508del. Currently available, disease-modifying, CF drugs work by rescuing the function of mutated CFTR (Cystic Fibrosis Transmembrane Conductance Regulator) anion channel. Recent research work shows that membrane lipids, and the cell lipidome in general, play a significant role in the mechanism of CFTR defective trafficking and, on the other hand, in its rescue. In this paper, by using untargeted lipidomics on CFBE41o- cells, we identified distinctive changes in bronchial epithelial cell lipidome associated with treatment with the triple combination VX-661/VX-445/VX-770 (drug name: Trikafta) and other CF drugs. Particularly interesting is the reduction of ceramide levels, known molecular players in the induction of apoptosis, that appears to be associated with a decrease in cell susceptibility to undergo apoptosis. This evidence could account for additional beneficial role of the triple combination on CF phenotypes.

Keywords

Cystic Fibrosis, Drugs, Trikafta, lipidomics, ceramides

Introduction

In the last five years, several studies investigated the role of lipid composition and dynamics of the plasma membrane in the trafficking of CFTR, the anion transporter defective in cystic fibrosis. The role of cholesterol and ceramides, including short chain ones (1), in the formation of CFTR clusters in the plasma membrane has been reported (2), as well as the stabilization of CFTR triggered by phosphatidylserines (PS)(3). An important contribution to CFTR stability at the cell membrane also comes from the action of flippases (4), enzymes known to regulate the movement of phospholipids across the cell membrane. Very recently, Bear's group demonstrated that membrane cholesterol plays a significant role in the activity of CFTR (5). Despite these work clearly

demonstrate a crucial role of lipid composition in CFTR trafficking and activity, the CF scientific community currently lacks an untargeted lipidomic profiling of CF-relevant cell models, non-limited to some selected lipid species, but directed toward the whole lipidome. High-resolution liquid chromatography-mass spectrometry (LC-MS) represents a key resource for untargeted lipidomics, thanks to the possibility to identify and quantify hundreds of individual lipid species in biofluids, cells and tissues(6). Lipidomics has been applied to many different human tissues like brain (7, 8), liver (9), kidney (10) and lungs (11). Quite surprisingly, compared to other "omes" (12, 13), the lipidome of the human bronchial epithelium (BE) has been less investigated. Few papers describe analytical efforts in lipidomics directed toward BE (14), while most of the lipidomics work associated with CF research has been done on profiling and biomarker discovery in both plasma (15, 16) and BAL fluid (17, 18). At cellular level, a successful CFTR rescue maneuver, beside promoting a better folding and trafficking of CFTR, might be linked to significant changes in the overall lipid composition of the cell membranes, that could either favor or contrast the rescue itself. Several studies have partially addressed this point: a positive impact of pharmacological modulation of the messaging action of sphingolipids on CF pathology has been proposed with the recent works on S1P signaling pathway (19, 20). On the contrary, a negative impact on CFTR half-life at the plasma membrane has been postulated for chronic co-administration of the potentiator ivacaftor (VX-770) and the corrector lumacaftor (VX-809) (21, 22). Works focused on F508-del, the most frequent CFTR mutation, suggested that VX-770 could either destabilize VX-809-corrected F508del-CFTR, thus markedly increasing mutant protein turnover rate (21) or decrease the folding efficiency and metabolic stability of VX-809-rescued F508del-CFTR at the endoplasmic reticulum (ER) and post-ER compartments, thus causing reduced cell surface F508del-CFTR density and function [22]. All this work and evidence point at a crucial role of lipid composition on CFTR physiology. On these premises, we conducted an extensive untargeted lipidomics investigation of immortalized F508del human bronchial epithelial cells (CFBE41o-) treated with some of the drugs (and combination) currently available for CF patients, including the recently introduced Trikafta. It consists of two correctors having different mechanism of action, VX-661 or tezacaftor and VX-445 or elexacaftor, plus VX-770 as potentiator (23). The aim of the current work is to extensively profile the lipidomic content of the F508del-CFTR human bronchial epithelium, in relation to successful CFTR pharmacological rescue maneuvers.

We hypothesize that the treatment with these drugs, the improved trafficking and expression at the plasma membrane of mutant CFTR might be associated with specific changes in the lipidomic profile of CFBE cells, partially restoring or rebalancing the altered lipid composition.

Results

Over a period of 2 months, we established and maintained six independent CFBE cell preparations and we incubated them with corrector VX-809 (Lumacaftor), potentiator VX-770 (Ivacaftor) and drug combination VX-809/VX-770 (Orkambi) and VX-445/VX-661/VX-770 (Trikafta). DMSO was used as control incubation. For each of these incubations, CFTR rescue was verified as already described (24). After pelleting and lipid extraction, an extensive lipid profiling by high-resolution LC-MS was then performed on these samples. Including blank, procedure blank and quality check (QC) samples, and dual ESI+/ESI- data acquisition, a total of 220 analytical runs were performed. All the data generated from this sample set were then analyzed by multivariate data analysis (25), extracting all the observed features from all the experimental groups. The full features table is reported as Supporting Datafile 1. We then used both unsupervised (Principal Component Analysis – PCA) and supervised (Partial Least Squares Discriminant Analysis – PLS-DA) analysis methods, with the aim to identify changes in the global lipidomic profiles. The Principal Component Analysis (PCA) revealed a clear (but trivial) separation between the groups and blank runs (Figure S3 in Supplementary Datafile), but also revealed differences between the five experimental groups, particularly over PC1 Vs PC3 and PC 2 Vs PC3 (Figure S4). The Partial Least Square Discriminant Analysis (PLS-DA) revealed a clear separation between the control group lipidome (DMSO) and that of CFBE cells treated with the drugs (Figure 1). We then checked our model for overfitting as recommended for untargeted metabolomics experiments (26). Figure S5 reports the results of this check and demonstrates that the PLS-DA model is reliable. The PLS-DA scores plot, accounting for 26% of the total variability observed in the dataset, shows that: 1) the observed differences between the experimental groups exceed the observed variability between the different biological replicates, represented by the spreading of the dots within the same group. 2) Each drug or combination imparts peculiar changes to the cell lipidome, in a way that each experimental group appears separated from the others. We then extracted the data for the top 75 features

contributing the most to the observed group separation (Variable Importance in Projection – VIP features). Figure S6 shows the relative abundance of each feature (provisionally identified with a retention time/mass-to-charge ratio: RT_m/z) in each of the experimental groups. With the same data matrix (75 features X 30 samples) we then performed a cluster analysis. The heatmap reported in Figure 2 shows that the samples, based on these 75 features, naturally cluster into 5 separate groups corresponding to the experimental ones. We then went back to the original data, with the aim to annotate these features. Each m/z ratio at a given RT value was extracted from the LC-MS runs, checked for consistency, deconvoluted for adducts and annotated using the publicly available LIPIDMAPS database (27). A total of 48 features out of 75 were annotated by positively assigning them to a lipid ID. Table 1 reports the list of the 48 lipids, divided by lipid category. Supporting Datafile 2 reports the final list of lipids and their peak areas in each sample. Figure S7 shows the corresponding PCA scores plot. These annotated data were then used to confirm the sample clustering into the original experimental groups (Figure 3, Panel A) and to search for patterns of correlation among the annotated species (Figure 3, Panel B). Based on this analysis, two major clusters of lipids were observed. We thus performed a pathway analysis using the lipids belonging to these two clusters. As reported in Figure S8, while lipids for cluster 1 (Panel A) mostly belong to glycerophospholipid metabolism (GP), the most enriched pathway in cluster 2 is sphingolipid metabolism (SL, Panel B). These results indicate that two among the most important metabolic pathways for lipids (GP and SL) are involved in the cellular response of F508del-CFTR expressing CFBE41o- to the tested drugs. The multivariate data analysis scenario reported so far refers to a simultaneous comparison of all the tested groups taken all together, i.e. a general overview of the lipidomic response of the model to CFTR rescue. In order to have a picture of the distinctive changes associated with the treatment with each single drug or combination, we also performed binary comparisons with each experimental group versus the control. All the significant features were again annotated (Supporting Datafile 3).

Role of VX-770

Given the results reported in Figure 1, suggestive of an effect of VX-770 in the overall changes observed in the lipidomic signatures, we then specifically investigated the molecular changes associated with this drug. Indeed,

Bear's group already demonstrated (28) that VX-770 interacts with membrane lipid structures, increasing membrane fluidity. We thus interrogated our untargeted dataset by comparing the annotated lipids observed in all the binary comparisons involving VX-770. Figure 4 shows the up/downregulated lipids, along with the corresponding Venn diagram highlighting the overall data overlap between the groups. Interestingly, while the treatment with Trikafta appears to have the biggest impact on the global lipidomic changes of this model, with 39 altered molecules, 8 individual lipids (a ceramide, 4 polyunsaturated phosphatidylcholines and 3 polyunsaturated alkenyl-phosphatidylcholines) are present at the intersection between all the 3 groups and appear thus to be associated with VX-770. These molecules, reported in Table S1, are downregulated in all VX-770 groups compared to control. Phosphatidylcholines are among the major components of membrane lipids (29) and have a huge impact on the mechanical and biophysical properties of the membrane itself (30, 31). Changes in their metabolism (increased turnover rate) have been associated (32) with the altered membrane recycling observed in CF. These phospholipids also constitute the largest lipid component of BAL fluid in CF patients (33). On the other hand, PCs represent one of the largest lipid families, with 1773 individual PC species currently reported in the LipidMaps database. It is thus difficult to exactly pinpoint the reasons for the observed downregulation of these particular 7 lipids associated with VX-770. In 2017, it was demonstrated (34) that this drug restores the PC secretion mediated by ABCB4 membrane transporter. A (selective) increased secretion, perhaps mediated by other transporters, might be in line with the decrease of the individual PC we observed in the CFBE lipidome. The observed downregulated ceramide also appears intriguing. Ceramides too have been associated with the properties of cell membranes (35) and to the formation and structure of lipid rafts (36). The role of these sphingolipids in CF has been explored (37): ceramides are known to accumulate in CF epithelial cells, triggering inflammation and cell death (38). The decrease of 16:0 ceramide we observed in the VX-770 groups is thus consistent with the positive effect of this drug on the CF phenotype.

Focus on the triple combination (Trikafta)

Given the great expectations associated with Trikafta for the management of CF, we then focused our analysis on the binary comparison of the corresponding group with the control one. Control and Trikafta groups are already

separated by unsupervised PCA, as reported in Figure 5, Panel A, thus demonstrating that this drug alters the lipid profile of CFBE in a clearly detectable way. Following a subsequent t-test, with correction for multiple testing (adjusted p-value 0.05 FDR) we outlined those features changing by at least 1.5 fold in a statistically significant way (see the corresponding volcano plot, Fig. 5, Panel B). These lipids (37 down- and 22 upregulated with the treatment) are reported in Table S2. This dual comparison highlights some other interesting changes in the molecular composition of the CFBE lipidome. As reported in Figure S9, a general downregulation of ceramides in the untargeted dataset appears to be associated with the CFTR rescue promoted by Trikafta. To confirm this data and to evaluate the ceramide levels in all the groups, we performed a second targeted LC-MS/MS experiment, focusing on these 6 molecules (Figure 6), normally among the most abundant in mammalian tissues (39). This experiment showed that, while a trend for downregulation is observed also for VX-770 alone and combined VX-770/VX-890, the triple combination is the only treatment that lowers the levels of *all* six major ceramides simultaneously and in a statistically significant way. To investigate the biological relevance of the decrease in ceramide expression in bronchial cells, we evaluated the susceptibility of CFBE41o- cells to undergo apoptosis. It was indeed demonstrated that ceramides act as second messengers involved in the induction of apoptosis (40, 41) and that augmented ceramides levels are associated with lung endothelial and epithelial cell apoptosis in murine models exposed to cigarette smoke (42, 43). In addition, XM462, an inhibitor of ceramide biosynthesis, promotes cell survival (44). Thus, we reasoned that, by lowering ceramide levels, the triple combination VX-445/VX-661/VX-770 might decrease cell susceptibility to undergo apoptosis following exposure to submaximal pro-apoptotic stimuli. To this aim, CFBE41o- cells expressing F508del-CFTR were plated at low density on high-quality 96-well plates suitable for imaging. After 24 hr, the cells were exposed to different concentrations (1 – 10 μM) of etoposide, a topoisomerase II inhibitor able to induce apoptosis in bronchial cells (45), in the absence or in the presence of single or combined CFTR modulators. The following day, by means of counterstaining with Hoechst 33342 and propidium iodide, we evaluated the number of living cells (i.e. cells negative for propidium iodide staining) for each condition (Figure 7A). None of the CFTR modulators (as single drugs or as combinations) affected the count of viable cells under resting condition (i.e. in the absence of etoposide), demonstrating that CFTR modulators do not influence cell proliferation rate. On the contrary, treatment with

etoposide alone caused a dose-dependent decrease in the number of viable cells (Figure 7B). However, when etoposide was added to the cells in the presence of the triple combination VX-445/VX-661/VX-770, we consistently observed a higher number of viable cells as compared to wells treated with etoposide alone (Figure 7B). No other CFTR modulator or combination consistently affected cell counts. Taken together, these results demonstrate that the triple combination decreases cell susceptibility to undergo apoptosis following exposure to submaximal pro-apoptotic stimuli. This protective role might be associated with the downregulation of all six major ceramides observed following treatment with the triple combination (Fig. 6).

Less clear is the rationale for the downregulation of the three major LysoPCs observed in the untargeted (Figure S9). Beside their reported importance as possible CF biomarkers in some biofluids (15, 46), little is known about the role of these molecules in CF physiology. Among the many biological functions in which LysoPC are involved, these molecules are known to be secreted to attract macrophages (47). In addition to their signaling role, however, LysoPCs are *also* synthetic precursors: they are condensed with acyl-CoA to produce PCs and glycerophosphocholine to regulate membrane fluidity in mammalian cells (48). To better investigate this point, as we did for ceramides, we selectively measured these three lipids in CFBE cells by means of a targeted LC-MS/MS experiment. While the decrease in *all* six ceramides appeared to be associated with the treatment with Trikafta only, some of them were downregulated also following treatment with VX-809/VX-770 (Fig. 6). On the contrary, Figure 8, Panel A shows that the decrease of these lysoPCs is a *distinctive feature* of the treatment with the triple combination only. To gain a better picture of this point, we also measured the levels of these 3 LysoPCs in the supernatant of the same CFBE cells (triple combination Vs control only). Figure 8, Panel B shows that the decrease in the CFBE lipidome is associated with a *reduced consumption* of the same lipids from the incubation medium. This evidence allows to speculate that cells treated with the triple combination *simply use less* LysoPC from the medium to produce some of the PCs that are downregulated in triple combination cells (Table S1 and Supporting Datafile 3).

Discussion

Our work represents the first untargeted exploration of the changes in the global lipidomic profiles of the F508del-CFTR bronchial epithelial cells in response to CFTR rescue by drugs. The experiments were performed on independent cell cultures, established over a broad timeframe: our results thus incorporate a realistic biological variability. We demonstrated that each of the tested drugs and combination produces a characteristic set of changes in the cell lipidome that goes beyond the biological variability of different cell cultures. We showed that VX-770 treatment is associated with a particular lipid signature of 7 phosphatidylcholines and a ceramide. We then focused on the triple-drug combination (Trikafta), for which we observed a decrease of 6 ceramides. We confirmed this evidence in a second targeted experiment. This decrease in ceramide content is consistent with a beneficial effect of the drug caused *also* by a reduction of these proapoptotic stimuli, as demonstrated by a dedicated experiment on CFBE cells. We also show that the treatment with this drug combination is associated with a decrease of three LysoPC in the cell lipidome, with concomitant higher levels of these lipids in the supernatant. While the evidence is clear, a lot remains to explain in the balance of LysoPC metabolism in CF. In this paper, we speculate that our data suggest a reduced use of these LysoPC by Trikafta treated cells to trigger a particular lipid membrane remodeling. We are well aware that our untargeted survey, albeit generic and unbiased, still does not cover the whole cell lipidome. For many technical reasons, some lipid families are often under-represented in this kind of untargeted experiments. Future efforts might perhaps move on from our results to implement targeted profiling of individual lipid families. For example, phosphatidylinositols and their phosphates (PI and PIPx), very important signaling lipids known to be involved in CF (49), require dedicated sample preparation and analytical strategies and are thus virtually absent from our untargeted dataset. It should also be noted that our findings might be only partially translated to primary cells. Indeed, the clear lipidomic alterations we observed in immortalized bronchial cells might be less evident in primary cells, in particular when compared to interindividual variability. Our findings should thus deserve future larger scale confirmatory studies. We nevertheless believe that our study will represent a helpful dataset for future research. Looking ahead, if the crucial role of cell lipidome in CFTR rescue is confirmed, new scenarios will open up for the future of CF pharmacology. Strategies for lipidome remodeling might be used to enhance and support the pharmacological modulation of CFTR, thus ameliorating the CF phenotype and patient's status. The active modulation of the cell membrane

lipidome (MLT: membrane lipid therapy) has already been proposed for many different applications (50),(51),(52). Quite surprisingly, MLT has never been proposed for CF, perhaps because of a lack of knowledge of the specific lipidomic alterations induced by the disease. In this perspective, we are hereby sharing with the worldwide CF community this body of data and evidence, collected on the most widely used in-vitro cell line used to investigate CF pharmacology.

Materials and Methods

Chemicals, Reagents, Instruments and Analytical Standards.

2-Propanol (IPA) was purchased from VWR Chemicals (Milano, Italy), all other chemicals and reagents used for sample preparation and LC-MS/MS analysis were purchased from Aldrich (Milano, Italy). C17 Ceramide (d18:1/17:0) was purchased from Avanti Polar Lipids (Alabaster, Alabama USA). UPLC/MS and MS/MS systems and columns were from Waters (Milford, USA). VX-770, VX-809, VX-661 were purchased from SelleckChem (Houston, TX, USA).

Synthesis and characterization of VX-445

VX-445 was synthesized following a modified procedure reported by Haseltine, E. L. et al. (Patent: WO 2019/018395 Al). The full details of the synthesis and chemical characterization are described in the Supplementary Information file.

Cell Cultures and incubations

CFBE 41o- cells overexpressing F508del-CFTR were cultured until confluence, harvested, and prepared for untargeted lipidomics. To address the above described scientific questions, each F508del culture was then treated with vehicle alone (DMSO) or the following single drugs or combinations: VX-809 (3 μM), VX-661 (10 μM), VX-770 (5 μM), VX-445 (3 μM), VX-809/VX-770, VX-661/VX-770, VX-445/VX-770, VX-661/VX-445, VX-661/VX-445/VX-770. Six independent experiments were performed to ensure reproducibility. For each ~~individual~~

cell culture (5 million cells per condition), cells were harvested in PBS and pelleted. The concentration of VX-661 and VX-445 were chosen according to Keating et al. (23). Although VX-809 is not part of the newly developed combination drugs, we decided to test it because of the reported negative impact on CFTR half-life at the plasma membrane following chronic co-administration of VX-770 and VX-809 (21, 22). CFTR rescue was verified as recently described (24).

Evaluation of cell susceptibility to pro-apoptotic stimuli

CFBE41o- cells stably expressing F508del-CFTR were plated at low density (10,000 cell/well) on 96-well plates suitable for high-content imaging. After 24 hours, cells were treated with test compounds at the desired concentrations or with vehicle alone (DMSO), in the absence or in the presence of different concentrations (1 – 10 µM range) of etoposide to induce cell apoptosis. The following day plates were washed three times with D-PBS to remove dead cells, cell nuclei were counterstained with Hoechst 33342 and propidium iodide to visualized total and apoptotic cells, respectively. Plates were imaged with a 10X air objective using the Opera Phenix (PerkinElmer) high-content screening system. The excitation of Hoechst 33342 signal was at 405 nm and the emission at 435-480 nm. The propidium iodide signal was excited at 560 nm and the emission was measured at 570-630 nm. Data are expressed as means ± SEM, n = 8. Reproducibility of results was confirmed by performing three independent experiments. Statistical significance was tested by parametric ANOVA, followed by the Dunnet multiple comparisons test.

Lipid extraction

After trying the 3-phases Matyash (53) method, we observed that simpler 2-phase extraction with isopropanol yielded very similar results (see Figure S1 in Supplementary Datafile) but with a dramatically reduced time and effort. This method has already been demonstrated to produce adequate and repeatable lipid coverage for untargeted experiments (54). Cells pellets were thus resuspended with H_2O (50 µL), transferred to glass vials, and added with 1 mL isopropanol spiked with C17 Ceramide (1 µM) as internal standard. The samples were then vortexed for 10 minutes and sonicated for 10 minutes at room temperature (RT). The samples were then centrifuged at 20000 x g for 20 minutes and the supernatant (A) was carefully collected. Pellets were then re-

extracted with 100 µL of a mixture of methyl-tert-butyl ether (MTBE) /methanol (50:50 v/v), vortexed for 10 minutes and sonicated for 10 minutes at RT. After further 20 minutes centrifugation (20000 x g) the supernatant (B) was collected. Supernatants A and B were then pooled and dried under N_2. At the time of analysis, the lipid extracts were dissolved in 200 µL of methanol/chloroform (9:1, v/v) for untargeted LC-MS/MS analyses. All the samples, including procedure blanks, were extracted following this protocol. The whole sample set, consisting of a total of 64 samples, was then randomized, split into 4 batches and analyzed by high-resolution LC-MS, using the methods already optimized by our group for untargeted lipidomics [24-27]. For every batch a QC sample was prepared by pooling together 5 µL of all the samples of that batch, including blanks and procedure blanks. For each batch, QC samples, consisting of pools of all the samples of the batch (including blanks) were prepared and analyzed together with the samples within each batch (6 injections: at the beginning, at the end and in between the samples).

Untargeted LC-MS/MS analysis

The lipidomic analysis was carried out on a ACQUITY UPLC system coupled to a Synapt G2 QToF high-resolution mass spectrometer (Waters, Milford, MA, USA), acquiring both in positive (ESI+) and negative (ESI−) ion modes. Lipids separation was performed with a reverse-phase CSH C18 column (1,7 µm internal diameter; 2,1x50 mm, Waters). Eluents were acetonitrile/water (60:40 v/v) with ammonium formate 10 µM (A) and isopropanol/acetonitrile (90:10 v/v) with ammonium formate 10 µM (B). Injection volume was 3 and 5 µL for ESI+ and ESI- respectively. The flow rate was set on 0,450 mL/min, the column was kept at 50ºC, samples were eluted with the following gradient program: 0,0 -1,0 min 10 % B; 1,0 - 4,0 min 10 to 60 % B; 4,0 – 8,0 min 60 to 75 % B; 8,0 - 8,5 min 75 to 100 % B; 8,5 - 10,0 min 100 % B and 10,0 - 10,1 back to 10 % B. The column was then reconditioned for 1,9 min. The total run time was 12 min. Scan range was set from 50 to 1200 m/z. Cone voltage was set at 35 V. Source temperature was set to 90 ºC, desolvation gas and cone gas (N_2) flows were set to 800 and 50 L/h respectively, desolvation temperature was set to 400 ºC. Data were acquired in MSE mode, alternating MS and MS/MS scans (55). The scan time was set to 0.3 s, low collision energy was set to 4 eV and

high collision energy was ramped from 25 to 45 eV. Leucine enkephalin (2 ng/mL) was infused as lock mass for real-time spectra recalibration. Masslynx software (from Waters) was used for data acquisition.

Targeted ceramide and lysoPC analysis

Ceramides were also quantified in a targeted experiment, by using a triple-quadrupole instrument (Xevo-TQMS, Waters) coupled to a ACQUITY UPLC (Waters) chromatographic system, following the method already published by our group (39). The three Lyso PCs were quantified by using the same general LC-MS/MS method and adding the three corresponding MRM experiments (496→184, 524→184 and 52→184 for Lyso PCs 16:0, 18:0 and 18:1 respectively). Collision energy was set to 25 eV and cone voltage was set to 30V.

Data Analysis

The observed features for both ESI+ and ESI- polarities were extracted from the RAW data, integrated and realigned over all the runs by using the Markerlynx software (Waters, Inc.). The following parameters were used: mass range from 200 to 1200 m/z, retention time (RT) range from 1 to 10 minutes, minimum intensity 4000 ion counts, m/z tolerance for extracted ion current 0.03 m/z, RT tolerance 0.03 min. Background ions observed in procedure blank and blank runs above the same threshold were automatically excluded by the software (background exclusion list). Exogenous d18:1/17:0 ceramide was set as internal standard, observed as $[M\text{-}H_2O+H]^+$ and $[M+HCOO]^-$ adducts for ESI+ and ESI- ion modes respectively with RT 5.47±0.03 min. Although cell pellets were washed with PBS before extraction, the m/z values of the drugs were excluded from the peak picking process. All the samples from all the four acquisition batches were realigned using this ceramide as reference. The obtained datasets for ESI+ and ESI- were then merged in a final (1571 features X 42 samples) data matrix and analyzed using Metaboanalyst (56) web-based software. After passing the data integrity check, missing values (empty cells) in the data were automatically replaced with the minimum value of each given feature in the corresponding column. The dataset was then normalized by the sum of all the observed features, log transformed and Pareto scaled (57). The absence of instrumental response drift in the data was then verified, by checking the clustering of the QC samples within each batch (see Figure S2). As reported in the text, both PCA and PLS-DA analyses were then performed. Cross validation of PLS-DA analysis was performed by using the leave-one-out

algorithm (26) searching over 5 principal components. Q2 value was used as a benchmark of potential overfitting. Variable Importance in Projections (VIP) score for PLS-DA was calculated over component 1. Cluster analysis was done using heatmaps, by applying Euclidean distance measurement and Ward algorithm (56) to normalized data. Correlation analysis among the features was performed using Pearson r as distance measure (58). Pathway analysis was performed on annotated data, using their HMDB (59) identifier. Hypergeometric test was used for overrepresentation analysis and Relative-betweeness Centrality was used for Pathway Topology Analysis on the KEGG (60) pathway library for Homo Sapiens.

Feature annotation

The relevant features, provisionally indicated by a RT_m/z value and selected from VIP scores and t-tests from volcano plot analysis, were manually annotated. The corresponding m/z value at the given RT was first manually extracted from the RAW data. The observed accurate mass value was then searched against the LipidMaps database (27). The following adduct species were searched: $[M+H]^+$, $[M-H_2O+H]^+$, $[M+NH_4]^+$, $[M+Na]^+$ for ESI+ and $[M-H]^-$, $[M+HCOO]^-$ for ESI-, allowing 0.01 m/z as maximum allowed tolerance for both polarities. The resulting list of proposed matches was then manually scrutinized, considering the consistency of the proposed structures with the observed RT (based on the well-known chromatographic behavior of lipids in reversed-phase mode (61)) and with the observed MS/MS spectrum obtained in MSe mode for the given feature. None of the proposed annotations was confirmed with the use of an authentic analytical reference standard, so, based on current guidelines for reporting data in metabolomics (62, 63), the identification level of the lipids under investigation should be considered higher than 1. Lipid IDs should thus be considered putative throughout the text. For most of the proposed structures, we prefer not to make inferences on the exact composition of the fatty acyl chains and we thus report the condensed structure, for example DG(34:1) instead of DG(16:0/18:1).

Statistics

For binary comparisons, volcano plot analysis was used to select features based on their observed fold change between the two groups (≥ 1.5) and their FDR adjusted p-value based on a t-test ($p<0.05$). For univariate data

analysis, both 2 tailed unpaired t-test and one way analysis of variance (ANOVA) were performed using GraphPad Prism (GLS Biotech). Dunnett post –hoc test was used to compare all groups with each other.

Study Approval

This study was performed on immortalized human cell lines it thus does not need approval from ethical committee. All the experiments were performed in accordance to common guidelines for cell culture.

Authors contribution

NL, EP, CB and SMB performed all the experimental activities; AG synthesized VX-445; TB contributed to the data interpretation; NP supervised the biological assays; AA conceived the project, supervised the work and wrote the manuscript with the help of NP.

Acknowledgments

This work was supported by Italian Cystic Fibrosis Foundation grants FFC 1/2018 and FFC 1/2019 to A.A. and FFC #9/2019 to NP (with the contribution of "Delegazione FFC di Genova con Gruppo di sostegno FFC di Savona Spotorno", "Delegazione FFC di Valle Scrivia Alessandria", "Delegazione FFC di Montescaglioso", and "Delegazione FFC di Ascoli Piceno"). This work was also supported by Italian Cystic Fibrosis Foundation grant "Task Force for Cystic Fibrosis" to TB. Work in NP lab is also supported by the Italian Ministry of Health through Cinque per mille and Ricerca Corrente (Linea1).

Supplementary Materials

All the supplementary Materials are enclosed to the present submission

Data Availability

All the RAW datafiles related to this study are publicly available through the Metabolights (64) database. Raw files have been deposited to the EMBL-EBI MetaboLights database with the identifier MTBLS1480. The complete dataset can be accessed here https://www.ebi.ac.uk/metabolights/MTBLS1480.

REFERENCES

1. Caohuy H, Yang Q, Eudy Y, Ha TA, Xu AE, Glover M, Frizzell RA, Jozwik C, and Pollard HB. Activation of 3-phosphoinositide-dependent kinase 1 (PDK1) and serum- and glucocorticoid-induced protein kinase 1 (SGK1) by short-chain sphingolipid C4-ceramide rescues the trafficking defect of DeltaF508-cystic fibrosis transmembrane conductance regulator (DeltaF508-CFTR). *J Biol Chem.* 2014;289(52):35953-68.
2. Abu-Arish A, Pandzic E, Kim D, Tseng HW, Wiseman PW, and Hanrahan JW. Agonists that stimulate secretion promote the recruitment of CFTR into membrane lipid microdomains. *J Gen Physiol.* 2019;151(6):834-49.
3. Hildebrandt E, Khazanov N, Kappes JC, Dai Q, Senderowitz H, and Urbatsch IL. Specific stabilization of CFTR by phosphatidylserine. *Biochim Biophys Acta Biomembr.* 2017;1859(2):289-93.
4. van der Mark VA, de Jonge HR, Chang JC, Ho-Mok KS, Duijst S, Vidovic D, Carlon MS, Oude Elferink RP, and Paulusma CC. The phospholipid flippase ATP8B1 mediates apical localization of the cystic fibrosis transmembrane regulator. *Biochim Biophys Acta.* 2016;1863(9):2280-8.
5. Chin S, Ramjeesingh M, Hung M, Ereno-Oreba J, Cui H, Laselva O, Julien JP, and Bear CE. Cholesterol Interaction Directly Enhances Intrinsic Activity of the Cystic Fibrosis Transmembrane Conductance Regulator (CFTR). *Cells.* 2019;8(8).
6. Hu T, and Zhang JL. Mass-spectrometry-based lipidomics. *J Sep Sci.* 2018;41(1):351-72.
7. Ferrer I. Proteomics and lipidomics in the human brain. *Handb Clin Neurol.* 2018;150(285-302.
8. Astarita G, Stocchero M, and Paglia G. Unbiased Lipidomics and Metabolomics of Human Brain Samples. *Methods Mol Biol.* 2018;1750(255-69.
9. Clugston RD, Gao MA, and Blaner WS. The Hepatic Lipidome: A Gateway to Understanding the Pathogenes is of Alcohol-Induced Fatty Liver. *Curr Mol Pharmacol.* 2017;10(3):195-206.
10. Abbas I, Noun M, Touboul D, Sahali D, Brunelle A, and Ollero M. Kidney Lipidomics by Mass Spectrometry Imaging: A Focus on the Glomerulus. *Int J Mol Sci.* 2019;20(7).
11. Lv JP, Gao DY, Zhang Y, Wu DJ, Shen LH, and Wang XD. Heterogeneity of lipidomic profiles among lung cancer subtypes of patients. *J Cell Mol Med.* 2018;22(10):5155-9.
12. Braccia C, Tomati V, Caci E, Pedemonte N, and Armirotti A. SWATH label-free proteomics for cystic fibrosis research. *J Cyst Fibros.* 2019;18(4):501-6.
13. Balch WE, and Yates JR, 3rd. Application of mass spectrometry to study proteomics and interactomics in cystic fibrosis. *Methods Mol Biol.* 2011;742(227-47.
14. Zehethofer N, Bermbach S, Hagner S, Garn H, Muller J, Goldmann T, Lindner B, Schwudke D, and Konig P. Lipid Analysis of Airway Epithelial Cells for Studying Respiratory Diseases. *Chromatographia.* 2015;78(5-6):403-13.
15. Guerrera IC, Astarita G, Jais JP, Sands D, Nowakowska A, Colas J, Sermet-Gaudelus I, Schuerenberg M, Piomelli D, Edelman A, et al. A novel lipidomic strategy reveals plasma phospholipid signatures associated with respiratory disease severity in cystic fibrosis patients. *PLoS One.* 2009;4(11):e7735.
16. Ollero M, Astarita G, Guerrera IC, Sermet-Gaudelus I, Trudel S, Piomelli D, and Edelman A. Plasma lipidomics reveals potential prognostic signatures within a cohort of cystic fibrosis patients. *Journal of Lipid Research.* 2011;52(5):1011-22.
17. Seidl E, Kiermeier H, Liebisch G, Ballmann M, Hesse S, Paul-Buck K, Ratjen F, Rietschel E, and Griese M. Lavage lipidomics signatures in children with cystic fibrosis and protracted bacterial bronchitis. *J Cyst Fibros.* 2019.
18. Ma DC, Yoon AJ, Faull KF, Desharnais R, Zemanick ET, and Porter E. Cholesteryl esters are elevated in the lipid fraction of bronchoalveolar lavage fluid collected from pediatric cystic fibrosis patients. *PLoS One.* 2015;10(4):e0125326.

19. Malik FA, Meissner A, Semenkov I, Molinski S, Pasyk S, Ahmadi S, Bui HH, Bear CE, Lidington D, and Bolz SS. Sphingosine-1-Phosphate Is a Novel Regulator of Cystic Fibrosis Transmembrane Conductance Regulator (CFTR) Activity. *Plos One.* 2015;10(6).
20. Veltman M, Stolarczyk M, Radzioch D, Wojewodka G, De Sanctis JB, Dik WA, Dzyubachyk O, Oravecz T, de Kleer I, and Scholte BJ. Correction of lung inflammation in a F508del CFTR murine cystic fibrosis model by the sphingosine-1-phosphate lyase inhibitor LX2931. *Am J Physiol Lung Cell Mol Physiol.* 2016;311(5):L1000-L14.
21. Veit G, Avramescu RG, Perdomo D, Phuan PW, Bagdany M, Apaja PM, Borot F, Szollosi D, Wu YS, Finkbeiner WE, et al. Some gating potentiators, including VX-770, diminish Delta F508-CFTR functional expression. *Sci Transl Med.* 2014;6(246).
22. Cholon DM, Quinney NL, Fulcher ML, Esther CR, Das J, Dokholyan NV, Randell SH, Boucher RC, and Gentzsch M. Potentiator ivacaftor abrogates pharmacological correction of Delta F508 CFTR in cystic fibrosis. *Sci Transl Med.* 2014;6(246).
23. Keating D, Marigowda G, Burr L, Daines C, Mall MA, McKone EF, Ramsey BW, Rowe SM, Sass LA, Tullis E, et al. VX-445-Tezacaftor-Ivacaftor in Patients with Cystic Fibrosis and One or Two Phe508del Alleles. *N Engl J Med.* 2018;379(17):1612-20.
24. Pedemonte N, Bertozzi F, Caci E, Sorana F, Di Fruscia P, Tomati V, Ferrera L, Rodríguez-Gimeno A, Berti F, Pesce E, et al. Discovery of a picomolar potency pharmacological corrector of the mutant CFTR chloride channel. *Science Advances.* 2020;6(8):eaay9669.
25. Wehrens R. Chemometrics with R: Multivariate Data Analysis in the Natural Sciences and Life Sciences. *Use R.* 2011:1-281.
26. Szymanska E, Saccenti E, Smilde AK, and Westerhuis JA. Double-check: validation of diagnostic statistics for PLS-DA models in metabolomics studies. *Metabolomics.* 2012;8(Suppl 1):3-16.
27. Fahy E, Sud M, Cotter D, and Subramaniam S. LIPID MAPS online tools for lipid research. *Nucleic Acids Res.* 2007;35(Web Server issue):W606-12.
28. Chin S, Hung M, Won A, Wu YS, Ahmadi S, Yang D, Elmallah S, Toutah K, Hamilton CM, Young RN, et al. Lipophilicity of the Cystic Fibrosis Drug, Ivacaftor (VX-770), and Its Destabilizing Effect on the Major CF-causing Mutation: F508del. *Mol Pharmacol.* 2018;94(2):917-25.
29. Furse S, and de Kroon AIPM. Phosphatidylcholine's functions beyond that of a membrane brick. *Mol Membr Biol.* 2015;32(4):117-9.
30. Bhagat M, and Sofou S. Membrane Heterogeneities and Fusogenicity in Phosphatidylcholine-Phosphatidic Acid Rigid Vesicles as a Function of pH and Lipid Chain Mismatch. *Langmuir.* 2010;26(3):1666-73.
31. Szule JA, Fuller NL, and Rand RP. The effects of acyl chain length and saturation of diacylglycerols and phosphatidylcholines on membrane monolayer curvature. *Biophys J.* 2002;83(2):977-84.
32. Ulane MM, Butler JD, Peri A, Miele L, Ulane RE, and Hubbard VS. Cystic fibrosis and phosphatidylcholine biosynthesis. *Clin Chim Acta.* 1994;230(2):109-16.
33. Sahu S, and Lynn WS. Lipid composition of airway secretions from patients with asthma and patients with cystic fibrosis. *Am Rev Respir Dis.* 1977;115(2):233-9.
34. Delaunay JL, Bruneau A, Hoffmann B, Anne-Marie, Durand-Schneider, Barbu V, Jacquemin E, Maurice M, Housset C, Callebaut I, et al. Functional Defect of Variants in the Adenosine Triphosphate-Binding Sites of ABCB4 and Their Rescue by the Cystic Fibrosis Transmembrane Conductance Regulator Potentiator, Ivacaftor (VX-770). *Hepatology.* 2017;65(2):560-70.
35. Castro BM, Prieto M, and Silva LC. Ceramide: a simple sphingolipid with unique biophysical properties. *Prog Lipid Res.* 2014;54(53-67.
36. Bieberich E. Sphingolipids and lipid rafts: Novel concepts and methods of analysis. *Chem Phys Lipids.* 2018;216(114-31.
37. Grassme H, Riethmuller J, and Gulbins E. Ceramide in cystic fibrosis. *Handb Exp Pharmacol.* 2013216):265-74.
38. Becker KA, Riethmuller J, Seitz AP, Gardner A, Boudreau R, Kamler M, Kleuser B, Schuchman E, Caldwell CC, Edwards MJ, et al. Sphingolipids as targets for inhalation treatment of cystic fibrosis. *Adv Drug Deliver Rev.* 2018;133(66-75.
39. Basit A, Piomelli D, and Armirotti A. Rapid evaluation of 25 key sphingolipids and phosphosphingolipids in human plasma by LC-MS/MS. *Anal Bioanal Chem.* 2015;407(17):5189-98.
40. Chan C, and Goldkorn T. Ceramide path in human lung cell death. *Am J Respir Cell Mol Biol.* 2000;22(4):460-8.

41. Lavrentiadou SN, Chan C, Kawcak T, Ravid T, Tsaba A, van der Vliet A, Rasooly R, and Goldkorn T. Ceramide-mediated apoptosis in lung epithelial cells is regulated by glutathione. *Am J Respir Cell Mol Biol.* 2001;25(6):676-84.
42. Bodas M, Min T, and Vij N. Critical role of CFTR-dependent lipid rafts in cigarette smoke-induced lung epithelial injury. *Am J Physiol Lung Cell Mol Physiol.* 2011;300(6):L811-20.
43. Filosto S, Castillo S, Danielson A, Franzi L, Khan E, Kenyon N, Last J, Pinkerton K, Tuder R, and Goldkorn T. Neutral Sphingomyelinase 2. *American Journal of Respiratory Cell and Molecular Biology.* 2011;44(3):350-60.
44. Gagliostro V, Casas J, Caretti A, Abad JL, Tagliavacca L, Ghidoni R, Fabrias G, and Signorelli P. Dihydroceramide delays cell cycle G1/S transition via activation of ER stress and induction of autophagy. *Int J Biochem Cell Biol.* 2012;44(12):2135-43.
45. West KA, Brognard J, Clark AS, Linnoila IR, Yang X, Swain SM, Harris C, Belinsky S, and Dennis PA. Rapid Akt activation by nicotine and a tobacco carcinogen modulates the phenotype of normal human airway epithelial cells. *J Clin Invest.* 2003;111(1):81-90.
46. Chen AH, Innis SM, Davidson AG, and James SJ. Phosphatidylcholine and lysophosphatidylcholine excretion is increased in children with cystic fibrosis and is associated with plasma homocysteine, S-adenosylhomocysteine, and S-adenosylmethionine. *Am J Clin Nutr.* 2005;81(3):686-91.
47. Lauber K, Bohn E, Krober SM, Xiao YJ, Blumenthal SG, Lindemann RK, Marini P, Wiedig C, Zobywalski A, Baksh S, et al. Apoptotic cells induce migration of phagocytes via caspase-3-mediated release of a lipid attraction signal. *Cell.* 2003;113(6):717-30.
48. Yamashita A, Sugiura T, and Waku K. Acyltransferases and transacylases involved in fatty acid remodeling of phospholipids and metabolism of bioactive lipids in mammalian cells. *J Biochem.* 1997;122(1):1-16.
49. Himmel B, and Nagel G. Protein kinase-independent activation of CFTR by phosphatidylinositol phosphates. *EMBO Rep.* 2004;5(1):85-90.
50. Escriba PV. Membrane-lipid therapy: A historical perspective of membrane-targeted therapies - From lipid bilayer structure to the pathophysiological regulation of cells. *Biochim Biophys Acta Biomembr.* 2017;1859(9 Pt B):1493-506.
51. Mollinedo F, de la Iglesia-Vicente J, Gajate C, Estella-Hermoso de Mendoza A, Villa-Pulgarin JA, Campanero MA, and Blanco-Prieto MJ. Lipid raft-targeted therapy in multiple myeloma. *Oncogene.* 2010;29(26):3748-57.
52. Torok Z, Tsvetkova NM, Balogh G, Horvath I, Nagy E, Penzes Z, Hargitai J, Bensaude O, Csermely P, Crowe JH, et al. Heat shock protein coinducers with no effect on protein denaturation specifically modulate the membrane lipid phase. *P Natl Acad Sci USA.* 2003;100(6):3131-6.
53. Matyash V, Liebisch G, Kurzchalia TV, Shevchenko A, and Schwudke D. Lipid extraction by methyl-tert-butyl ether for high-throughput lipidomics. *J Lipid Res.* 2008;49(5):1137-46.
54. Sarafian MH, Gaudin M, Lewis MR, Martin FP, Holmes E, Nicholson JK, and Dumas ME. Objective Set of Criteria for Optimization of Sample Preparation Procedures for Ultra-High Throughput Untargeted Blood Plasma Lipid Profiling by Ultra Performance Liquid Chromatography-Mass Spectrometry. *Analytical Chemistry.* 2014;86(12):5766-74.
55. Wickramasekara SI, Zandkarimi F, Morre J, Kirkwood J, Legette L, Jiang Y, Gombart AF, Stevens JF, and Maier CS. Electrospray Quadrupole Travelling Wave Ion Mobility Time-of-Flight Mass Spectrometry for the Detection of Plasma Metabolome Changes Caused by Xanthohumol in Obese Zucker (fa/fa) Rats. *Metabolites.* 2013;3(3):701-17.
56. Chong J, Soufan O, Li C, Caraus I, Li S, Bourque G, Wishart DS, and Xia J. MetaboAnalyst 4.0: towards more transparent and integrative metabolomics analysis. *Nucleic Acids Res.* 2018;46(W1):W486-W94.
57. van den Berg RA, Hoefsloot HC, Westerhuis JA, Smilde AK, and van der Werf MJ. Centering, scaling, and transformations: improving the biological information content of metabolomics data. *BMC Genomics.* 2006;7(142.
58. Mondal S, and Mondal H. Value of r(2) in Statistical Analysis by Pearson Correlation Coefficient. *J Clin Diagn Res.* 2017;11(11):Cl1-Cl.
59. Wishart DS, Feunang YD, Marcu A, Guo AC, Liang K, Vazquez-Fresno R, Sajed T, Johnson D, Li C, Karu N, et al. HMDB 4.0: the human metabolome database for 2018. *Nucleic Acids Res.* 2018;46(D1):D608-D17.

60. Marco-Ramell A, Palau-Rodriguez M, Alay A, Tulipani S, Urpi-Sarda M, Sanchez-Pla A, and Andres-Lacueva C. Evaluation and comparison of bioinformatic tools for the enrichment analysis of metabolomics data. *BMC Bioinformatics.* 2018;19(1):1.
61. Cajka T, and Fiehn O. Comprehensive analysis of lipids in biological systems by liquid chromatography-mass spectrometry. *Trac-Trend Anal Chem.* 2014;61(192-206.
62. Schrimpe-Rutledge AC, Codreanu SG, Sherrod SD, and McLean JA. Untargeted Metabolomics Strategies-Challenges and Emerging Directions. *J Am Soc Mass Spectr.* 2016;27(12):1897-905.
63. Salek RM, Steinbeck C, Viant MR, Goodacre R, and Dunn WB. The role of reporting standards for metabolite annotation and identification in metabolomic studies. *Gigascience.* 2013;2(1):13.
64. Kale NS, Haug K, Conesa P, Jayseelan K, Moreno P, Rocca-Serra P, Nainala VC, Spicer RA, Williams M, Li X, et al. MetaboLights: An Open-Access Database Repository for Metabolomics Data. *Curr Protoc Bioinformatics.* 2016;53(14 3 1- 3 8.

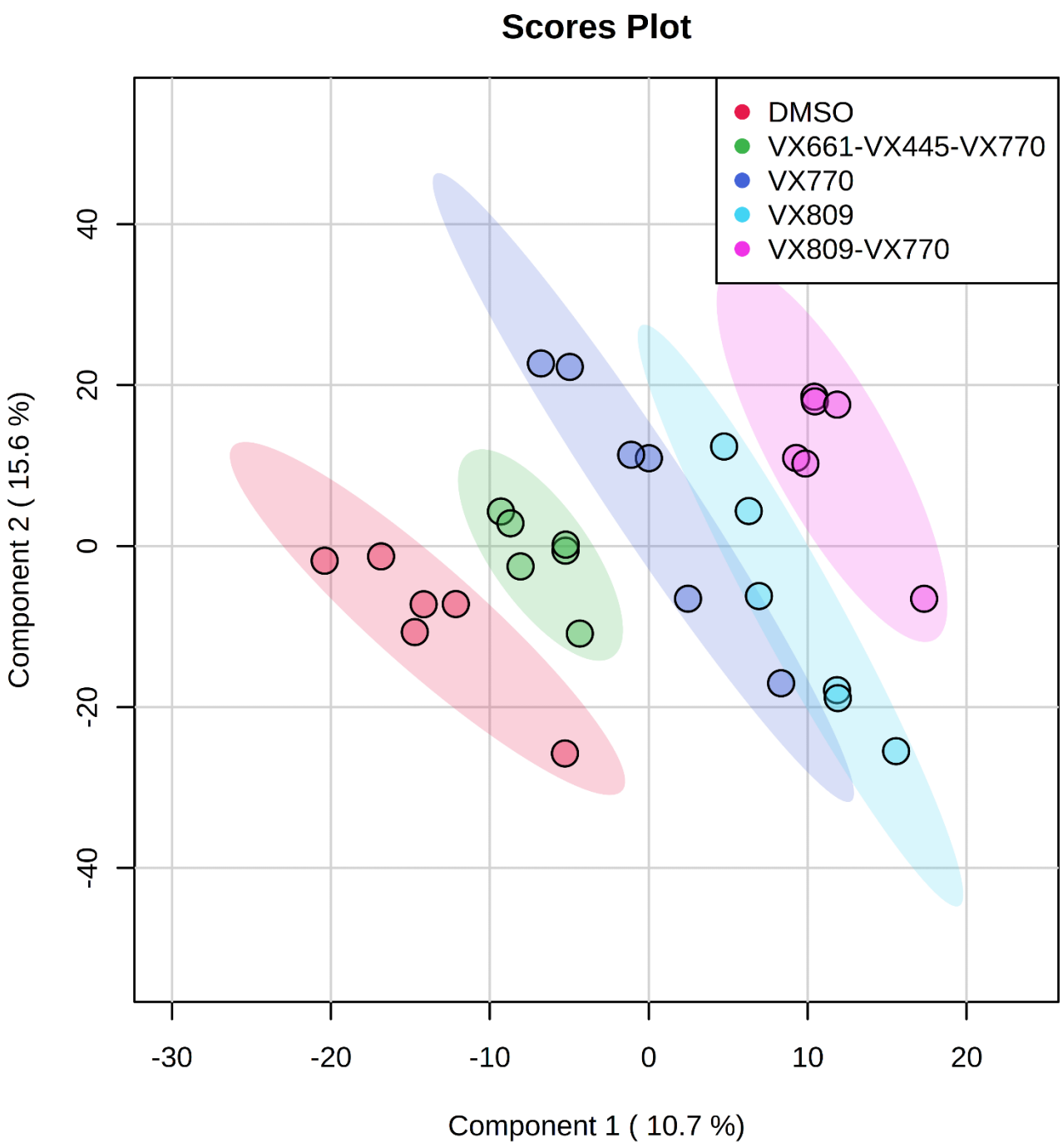

Figure 1: Scores Plot for PLS-DA analysis of CFBE cells lipidome treated with drugs or control DMSO. Blank and QC groups are omitted for clarity.

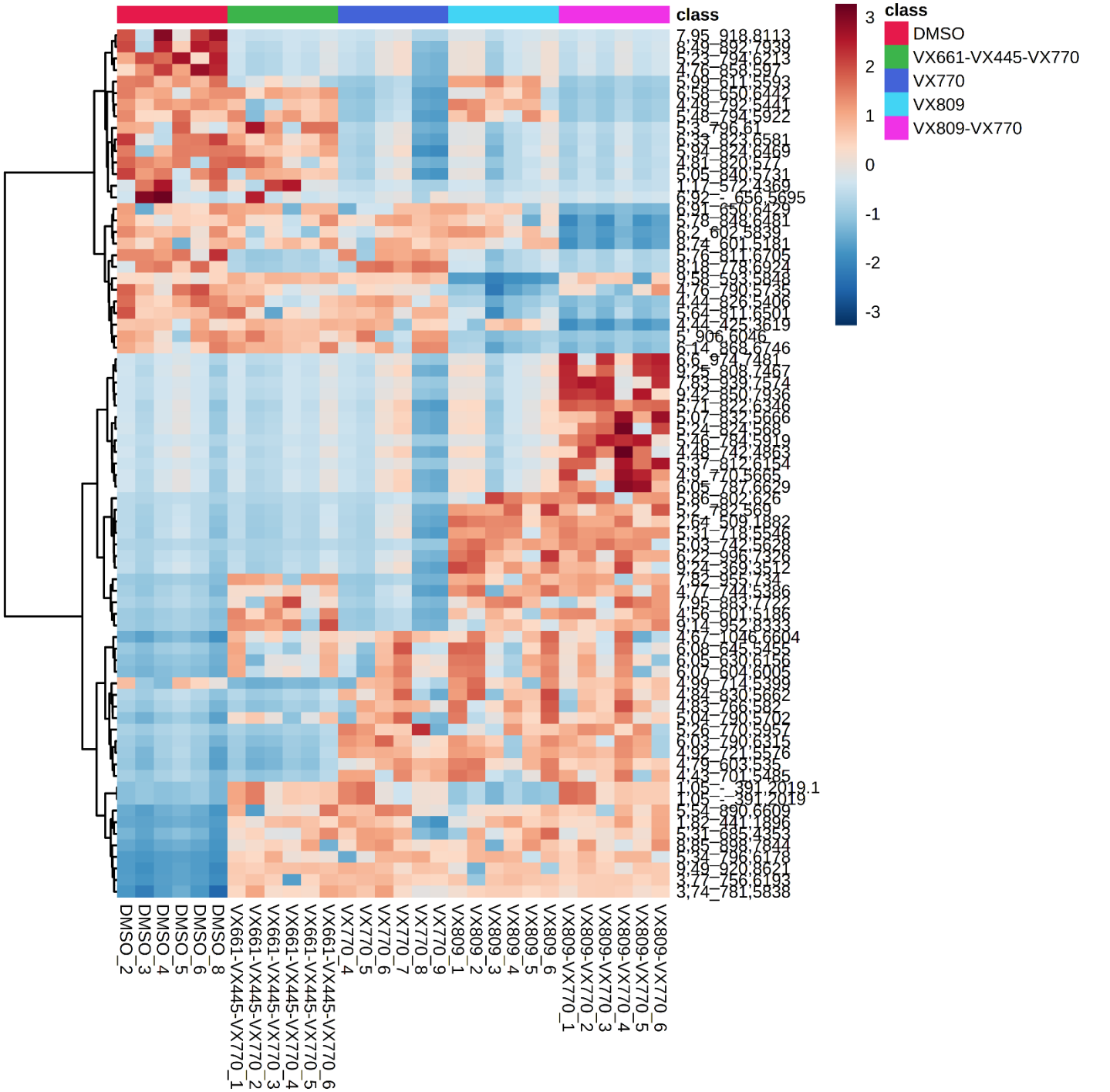

Figure 2: Heatmap for the clustering analysis of the CFBE lipidomics sample set. Based on the top 75 PLS-DA VIP features, the samples naturally cluster into the experimental groups.

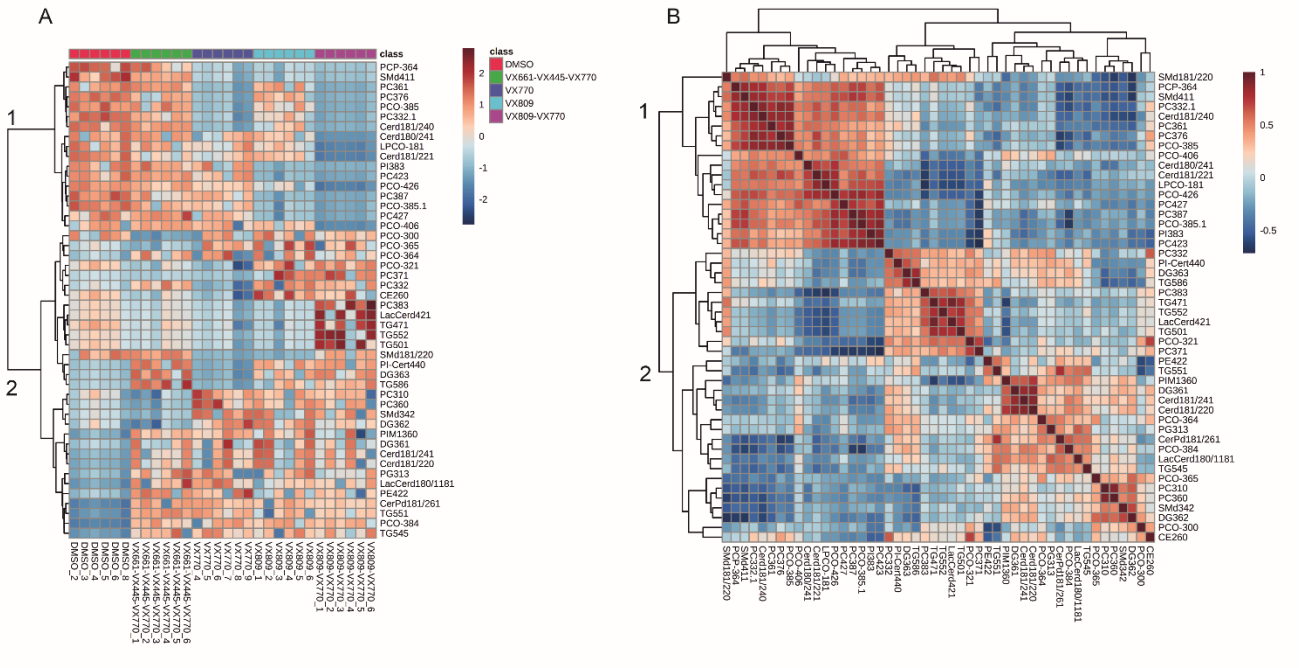

Figure 3: Correlation analysis for the 48 lipids. Panel A) Heatmap for the clustering analysis: based on the 48 PLS-DA VIP features, the samples naturally cluster into the experimental groups. B) Patterns of correlation among the 48 lipids. Two main clusters of lipids were observed in the dataset (1 and 2).

VX-445/661/770			
DOWNREGULATED		UPREGULATED	
Cer(d18:1/16:0)	Ceramide	Cer(d18:0/24:0)	Ceramide
Cer(d18:1/18:0)	Ceramide	LacCer(d18:1/14:0)	Ceramide
Cer(d18:1/20:0)	Ceramide	Cer(m18:0/18:0)	Deoxyceramide
Cer(d18:1/22:0)	Ceramide	Cer(m18:0/24:0)	Deoxyceramide
Cer(d18:1/22:1)	Ceramide	DG(38:2)	Diacylglycerol
Cer(d18:1/23:0)	Ceramide	DG(42:7)	Diacylglycerol
Cer(d18:1/24:0)	Ceramide	DG(44:7)	Diacylglycerol
Cer(d18:1/24:1)	Ceramide	PC(42:1)	Phosphatidylcholine
HexCer(d18:1/16:0)	Ceramide	PC(44:1)	Phosphatidylcholine
DG(32:0)	Diacylglycerol	PC(P-32:0)	Phosphatidylcholine
DG(32:1)	Diacylglycerol	PC(P-32:1)	Phosphatidylcholine
DG(34:1)	Diacylglycerol	PC(P-40:3)	Phosphatidylcholine
DG(34:2)	Diacylglycerol	PC(P 40:4)	Phosphatidylcholine
DG(38:4)	Diacylglycerol	PC(P-40:5)	Phosphatidylcholine
DG(38:6)	Diacylglycerol	PC(P-40:6)	Phosphatidylcholine
DG(O-34:1)	Diacylglycerol	PE(36:1)	Phosphatidylethanolamine
LysoPC(16:0)	Lysophosphatidylcholine	PE(P-33:0)	Phosphatidylethanolamine
LysoPC(18:0)	Lysophosphatidylcholine	PE(P-35:1)	Phosphatidylethanolamine
LysoPC(18:1)	Lysophosphatidylcholine	SM(d18:0/22:0)	Sphingomyelin
PC(32:2)	Phosphatidylcholine	SM(d18:0/24:0)	Sphingomyelin
PC(34:4)	Phosphatidylcholine	SM(d18:1/24:0)	Sphingomyelin
PC(36:4)	Phosphatidylcholine	TG(56:4)	Triacylglycerol
PC(36:5)	Phosphatidylcholine		
PC(36:6)	Phosphatidylcholine		
PC(37:6)	Phosphatidylcholine		
PC(38:7)	Phosphatidylcholine		
PC(42:10)	Phosphatidylcholine		
PC(P-30:0)	Phosphatidylcholine		
PC(P-36:4)	Phosphatidylcholine		
PC(P-36:5)	Phosphatidylcholine		
PC(P-38:6)	Phosphatidylcholine		
PE(36:5)	Phosphatidylethanolamine		
PE(40:5)	Phosphatidylethanolamine		
PE(P-38:6)	Phosphatidylethanolamine		
PS(40:6)	Phosphatidylserine		
SM(d18:1/14:0)	Sphingomyelin		
SM(d18:1/15:0)	Sphingomyelin		

VX-809/770	
DOWNREGULATED	
Cer(d18:1/16:0)	Ceramide
Cer(d18:1/20:0)	Ceramide
Cer(d18:1/23:0)	Ceramide
Cer(d18:1/24:1)	Ceramide
PC(32:2)	Phosphatidylcholine
PC(34:5)	Phosphatidylcholine
PC(36:5)	Phosphatidylcholine
PC(38:7)	Phosphatidylcholine
PC(40:7)	Phosphatidylcholine
PC(40:8)	Phosphatidylcholine
PC(42:10)	Phosphatidylcholine
PC(42:8)	Phosphatidylcholine
PC(P-36:4)	Phosphatidylcholine
PC(P-36:5)	Phosphatidylcholine
PC(P-38:6)	Phosphatidylcholine
PE(36:5)	Phosphatidylethanolamine
PE(P-38:6)	Phosphatidylethanolamine

VX-770			
DOWNREGULATED		UPREGULATED	
Cer(d18:1/16:0)	Ceramide	Cer(m18:0/18:0)	Deoxyceramide
DG(32:1)	Diacylglycerol	PC(P-40:3)	Phosphatidylcholine
DG(38:5)	Diacylglycerol	PC(P-40:4)	Phosphatidylcholine
DG(38:6)	Diacylglycerol	PI(38:4)	Phosphatidylinositol
PC(32:2)	Phosphatidylcholine		
PC(34:4)	Phosphatidylcholine		
PC(34:5)	Phosphatidylcholine		
PC(36:5)	Phosphatidylcholine		
PC(36:6)	Phosphatidylcholine		
PC(38:7)	Phosphatidylcholine		
PC(40:7)	Phosphatidylcholine		
PC(40:8)	Phosphatidylcholine		
PC(42:10)	Phosphatidylcholine		
PC(42:8)	Phosphatidylcholine		
PC(O-36:5)	Phosphatidylcholine		
PC(P-36:4)	Phosphatidylcholine		
PC(P-36:5)	Phosphatidylcholine		
PC(P-38:6)	Phosphatidylcholine		

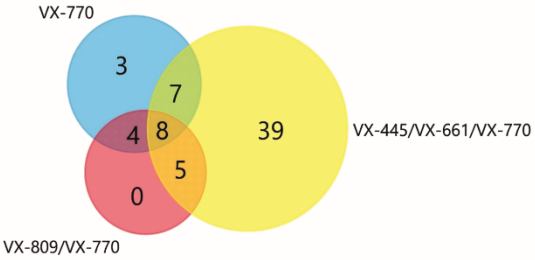

Figure 4: Significantly up and down regulated lipids observed in all the three VX-770 groups compared to control (FDR 0.05, FC>1.5) and corresponding Venn diagram of overlap. The 8 lipids indicated in red are at the intersection between the three groups.

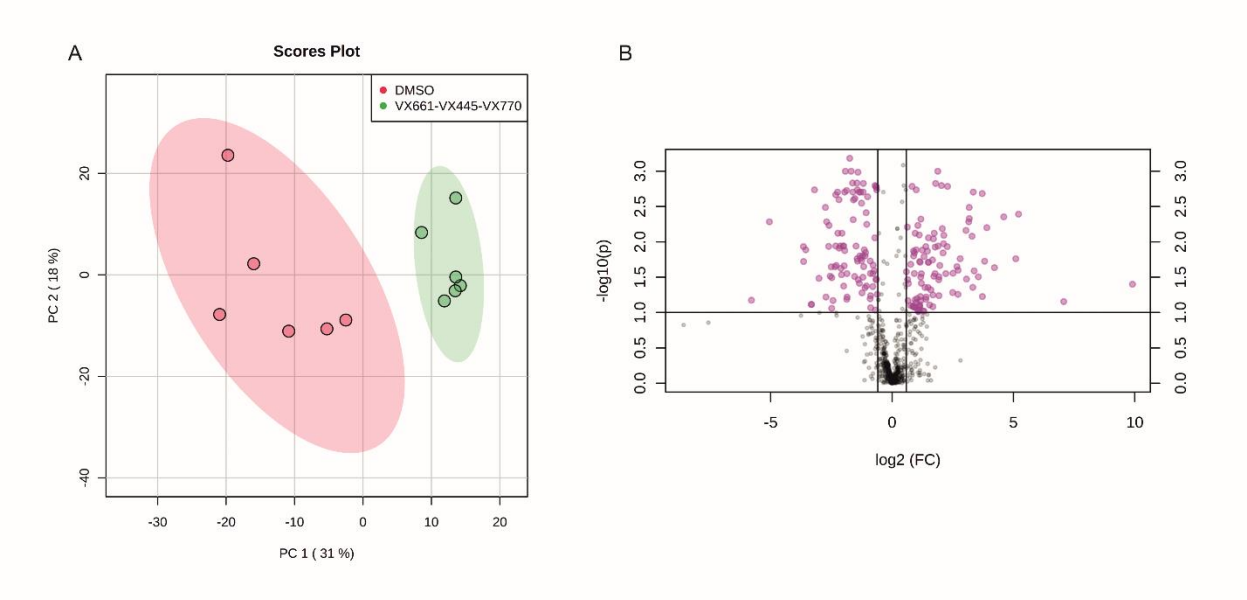

Figure 5: Panel A: PCA scores plot for the control/triple combination comparison. The two groups are separated in unsupervised data analysis. Panel B: Volcano plot for the same comparison, the features having a fold change greater than 1.5 (adjusted p-value 0.1 FDR) are indicated along with the regulation status following treatment with Trikafta.

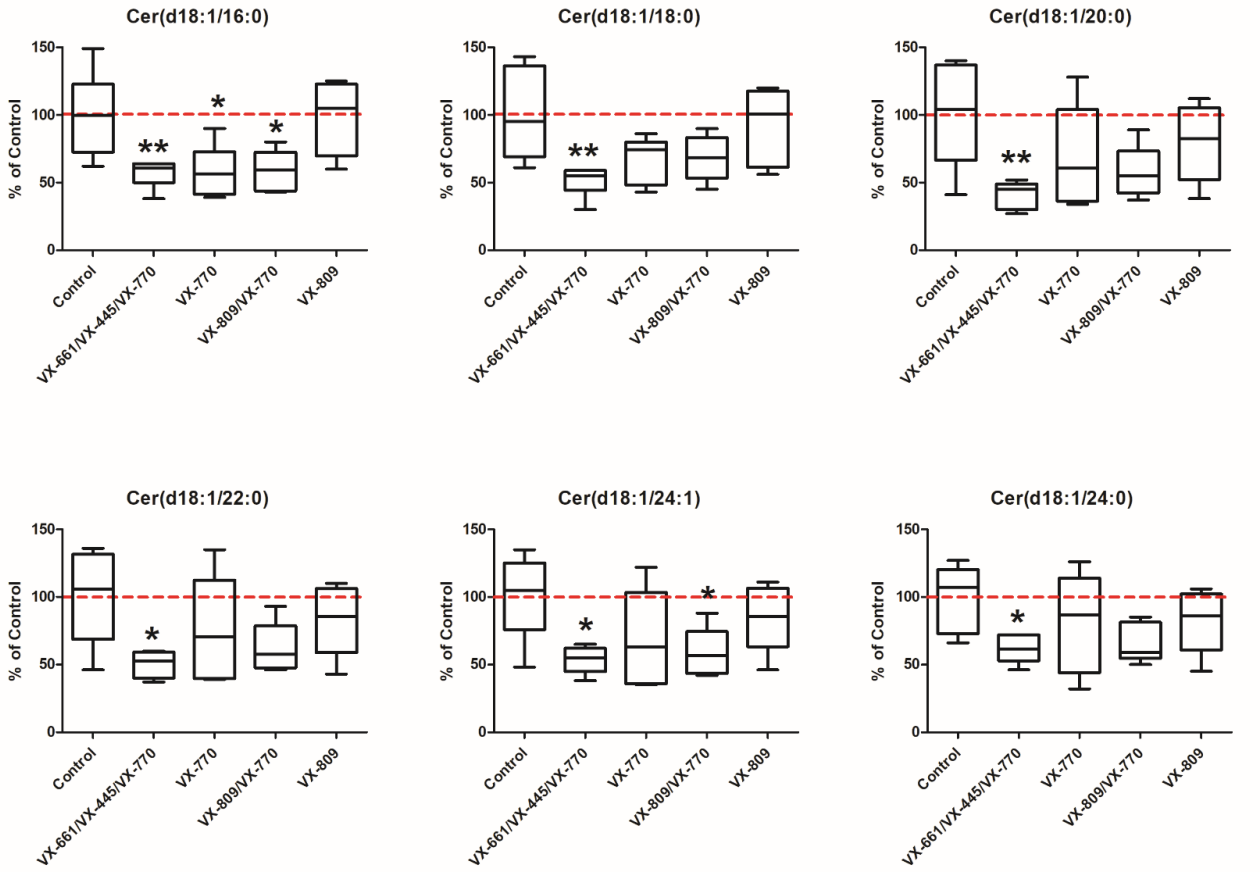

Figure 6: Targeted quantification of the 6 ceramides in all the experimental groups. * = $p < 0.05$ and ** = $p < 0.01$ compared to control in a one way-ANOVA test with Dunnett post-hoc test. The average level of the control group is represented by the dotted red line. Box and whiskers plot represent: the median value (inner bar), the 1st and 3rd quartile (box) and the minimum and maximum value (outer bars). Data represent mean±SEM, N=5.

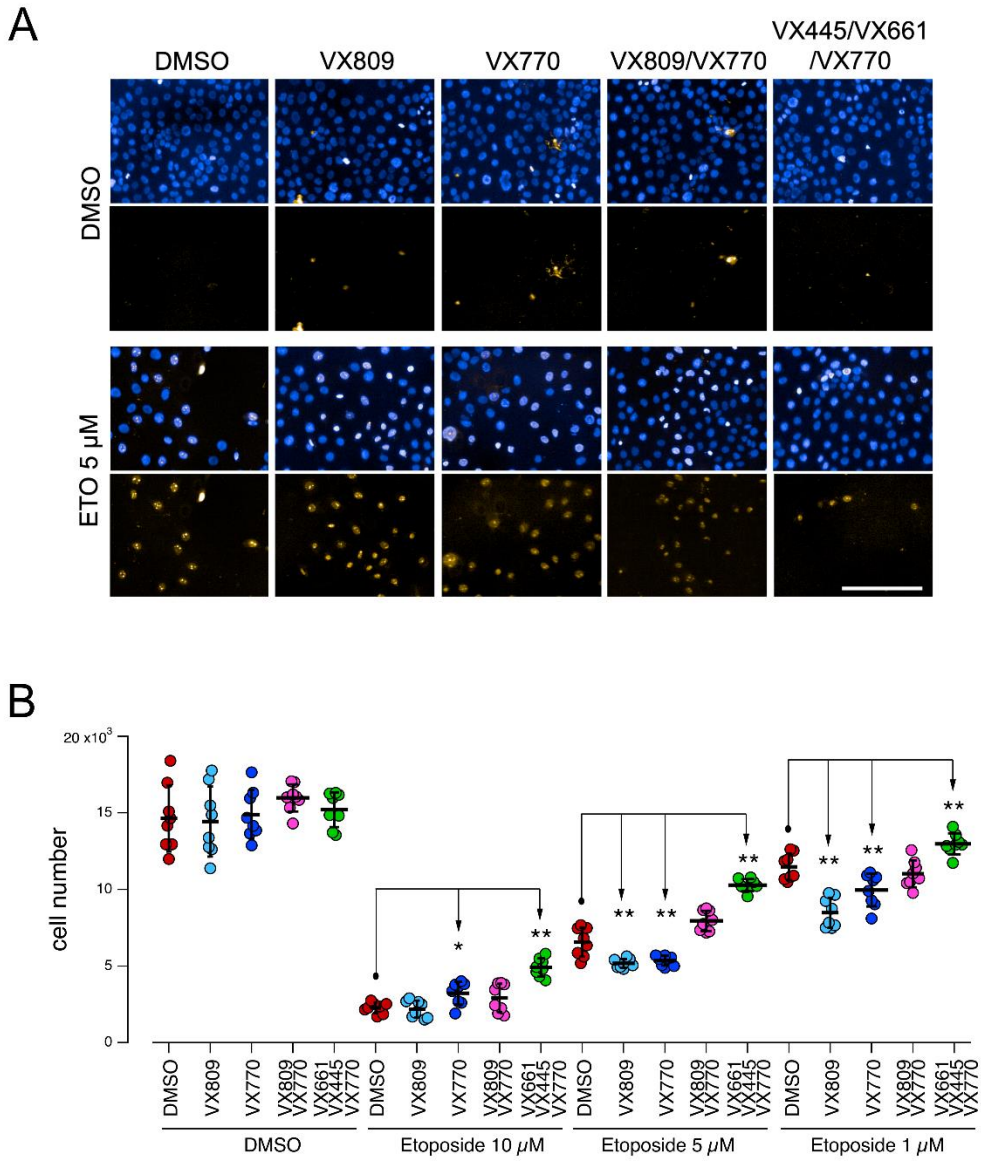

Figure 7: Susceptibility of bronchial cells treated with CFTR modulators to undergo apoptosis. CFBE41o- cells, were treated for 24 hr with vehicle alone or with the indicated concentrations of etoposide to induce apoptosis, in the absence or in the presence of the different CFTR modulators. Samples were then analyzed by means of automated high-content imaging and analysis. A. Representative images. Bar = 200 µm. B. quantification of the number of viable CFBE41o- cells per condition. * = $p < 0.05$ and ** = $p < 0.01$ compared to respective control (DMSO-treated) cells in a one way-ANOVA test with Dunnett post-hoc test. Data represent mean±SEM, N=5.

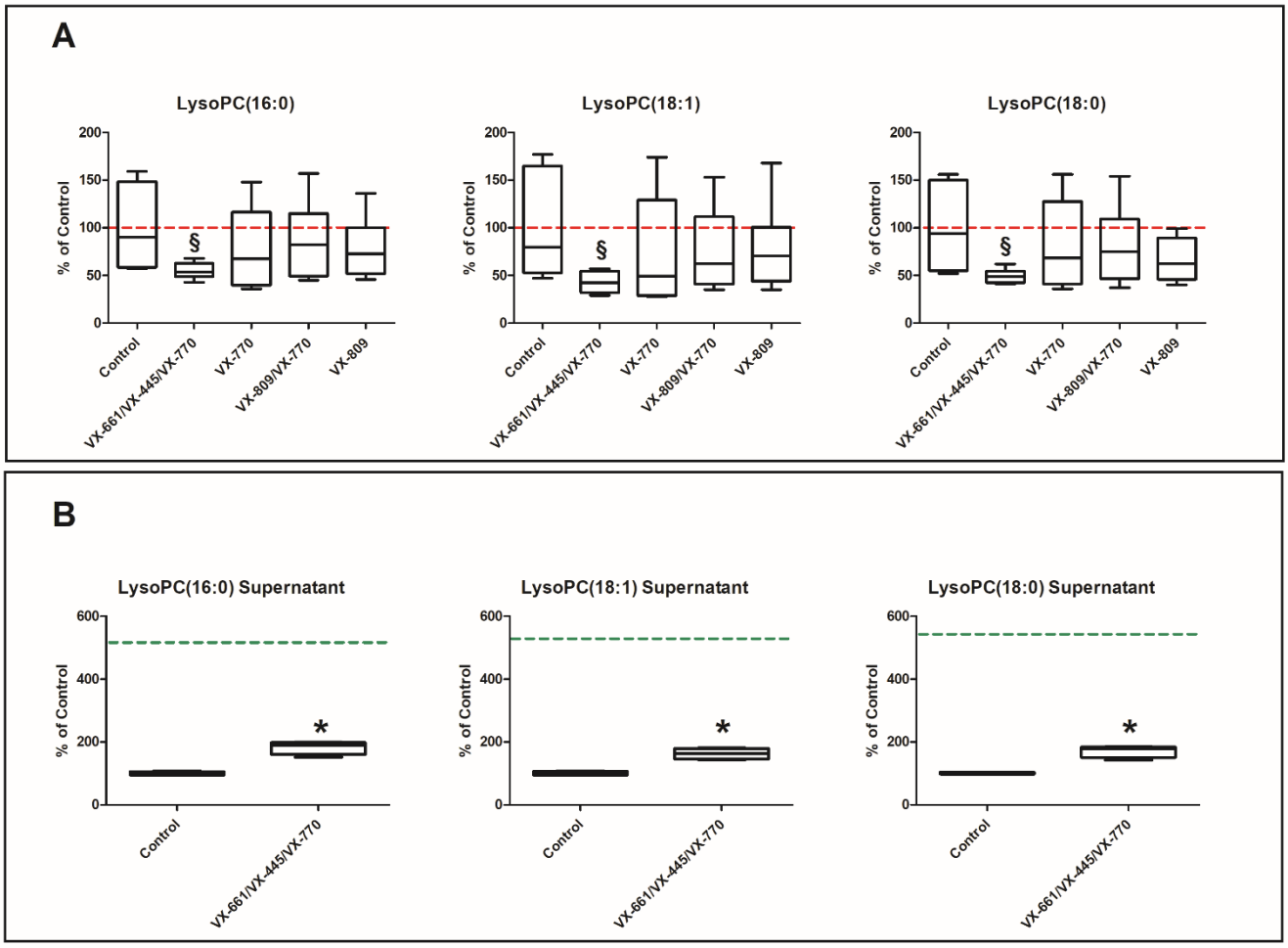

Figure 8. Targeted quantification LysoPCs in the CFBE cells. **Panel A**: LysoPC levels in lysates following treatment with the three drugs, 24 hours incubation; §= $p<0.05$ compared to control in a one way-ANOVA test with Dunnett post-hoc test. The average level of the control group is represented by the dotted red line. **Panel B:** LysoPCs levels in the supernatants of the same CFBE cells at 24 hours, following treatment with the triple combination; *= $p<0.05$ compared to control in a 2 tails t-test. The average level in the medium at the beginning of the incubation is indicated by the dotted green line. Box and whiskers plot represent: the median value (inner bar), the 1st and 3rd quartile (box) and the minimum and maximum value (outer bars). Data represent mean±SEM, N=5.

Sphingolipids	Phospholipids		Glycerolipids	Sterols
Cer(d18:0/24:1)	LPC(O-18:1)	PC(O-32:1)	DG(36:1)	CE(26:0)
Cer(d18:1/22:0)	PC(31:0)	PC(O-36:4)	DG(36:2)	
Cer(d18:1/22:1)	PC(33:2)	PC(O-36:5)	DG(36:3)	
Cer(d18:1/24:0)	PC(33:2)	PC(O-38:4)	TG(47:1)	
Cer(d18:1/24:1)	PC(36:0)	PC(O-38:5)	TG(50:1)	
CerP(d18:1/26:1)	PC(36:1)	PC(O-38:5)	TG(54:5)	
LacCer(d18:0/118:1)	PC(37:1)	PC(O-40:6)	TG(55:1)	
LacCer(d42:1)	PC(37:6)	PC(O-42:6)	TG(55:2)	
PI-Cer(t44:0)	PC(38:3)	PC(P-36:4)	TG(58:6)	
SM(d18:1/22:0)	PC(38:7)	PE(42:2)		
SM(d34:2)	PC(42:3)	PG(31:3)		
SM(d41:1)	PC(42:7)	PI(38:3)		
	PC(O-30:0)	PIM1(36:0)		

Table 1. The 48 annotated lipids, divided by lipid category